Using Leg Geometry to Align Androgenic Hair Patterns in Low Resolution Images for Criminal and Victim Identification

Frodo Kin-Sun Chan
School of Computer Engineering
Nanyang Technological University
Singapore
csfrodochan@ntu.edu.sg

Adams Wai-Kin Kong
School of Computer Engineering
Nanyang Technological University
Singapore
adamskong@ntu.edu.sg

***Abstract* — Identifying criminals and victims in digital media can be very challenging when neither their faces nor tattoos are observable. These criminals and victims can be masked gunmen, paedophiles, and victims in child pornographic images. Though skin marks and blood vessel patterns hidden in colour images have been proposed to address this problem, they have different limitations. Blood vessel patterns are not suitable for subjects with high concentration of body fat or melanin and skin marks are not suitable for the cases where only low resolution images are available. A recent paper pointed out that androgenic hair, which is also called body hair, and its follicles can be used as biometric traits and demonstrated that androgenic hair patterns in low resolution images are effective for personal identification. In that study, variations of viewpoints and poses were ignored, but these variations are unavoidable in real cases. To overcome the weaknesses of the previous method, this paper proposes an algorithm based on geometric information for aligning androgenic hair patterns on lower legs. The experimental results on 1,138 low resolution images from 283 different legs show that the proposed alignment algorithm offers more than 5% improvement.**

***Keywords* — Forensics, biometrics, skin marks, blood vessels**

I. INTRODUCTION

The popularity of digital media provides new challenges to law and enforcement agents around the world, since the significant number of child pornographic images and videos has been posted on the Internet. In Canada alone, 30,000 cases of child pornography had been reported [2]. Criminals are usually careful not to show their faces in child pornographic images. In addition to child pornography, identification of masked gunmen and terrorists is also a challenging problem to law enforcement agents.

To address these problems, skin marks and vein patterns have been studied [3-4]. However, some people have only limited skin marks on some of their body sites and some have high concentration of body fat or melanin, which makes visualizing vein patterns hidden in colour images difficult. Thus, new biometric traits for criminal and victim identification are still demanded.

Medical studies have implied that androgenic hair, which is commonly called body hair, and its follicles can be effective biometric traits. New follicles do not form naturally after birth in humans [5] and all body hairs manifest a cycle. When one hair falls out, another new hair will grow at the same follicle [5]. Androgenic hairs have a long hair cycle. For example, a complete cycle of androgenic hairs on legs can be up to one year [6]. Figs. 1(a) and (b) show two images from the same leg. Fig. 1(a) was collected in August 2009, while Fig. 1(b) was collected in October 2008. The colour circles in Figs. 1(a) and (b) show partial corresponding androgenic hair follicles. From this small area, more than 40 corresponding androgenic hair follicles can be found.

Recently, Su et al. [1] demonstrated that androgenic hair patterns in low resolution leg images have high potential to address the challenges mentioned before. However, their method overlooked the importance of alignment. Accurate alignment is always critical for matching suspects (e.g., released prisoners) in a given database with criminals or victims in evidence images because these images are collected in uncontrolled environments, where viewpoint and pose variations are unavoidable. This paper proposes an algorithm based on leg geometry to align androgenic hair patterns in low resolution leg images for criminal and victim identification. According to our best knowledge, no one studied this issue before.

Image alignment methods can be classified into two categories — intensity-based and feature-based methods. The intensity-based methods directly search the best matched regions defined by an intensity-based similarity metric in two images. The feature-based methods search correspondences between two images through features extracted from them. Many feature detectors, including Harris detector [7], SIFT [8], PCA-SIFT [9] and SURF [10], have been considered. They, relying on distinctive features, e.g., strong edges, are not suitable for leg image alignment because each point on leg boundaries is similar and androgenic hairs in low resolution images do not form distinctive edges. Therefore, it is difficult to obtain corresponding points, particularly in low resolution images. The algorithm presented in this paper uses edge samples on leg boundaries for alignment and it does not rely on the distinctive feature points, which may not be obtained in

low resolution images. The geometric information employed by the proposed algorithm is always observable even in low resolution images.

The rest of this paper is organized as follows. Section II gives the preprocessing step. Section III presents the proposed alignment algorithm. Section IV describes the feature extraction and matching methods proposed by Su et al. [1] for evaluation and comparison. Section V reports the experimental results. Finally, Section VI offers some conclusive remarks.

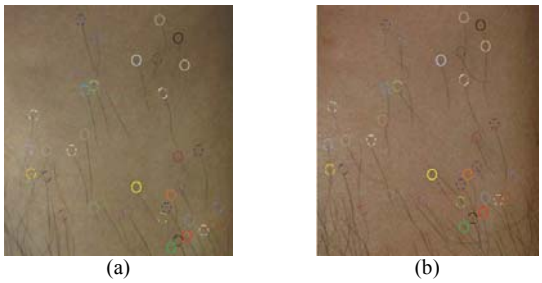

(a) (b)

Fig. 1. Illustration of the stability of androgenic hairs. (a) was collected in August 2009, while (b) was collected in October 2008.

II. The Preprocessing Step

Before leg images are inputted to the proposed alignment algorithm, a region of interest is extracted first. Fig. 2 illustrates the preprocessing step. Initially, the lower leg is captured (Fig. 2(a)). The region of interest is defined by six edge points, A, A', M, M', B, and B' (Fig. 2(b)). To find the lines AA' and BB', the line MM', whose horizontal distance is the longest, is extracted. Once the line MM' is found, the lines AA' and BB' can be obtained by searching the shortest lines above and below MM'. Finally, the preprocessed image is segmented based on the region of interest, which is defined by A, A', M, M', B, and B'. This segmentation process is semi-automatic. If the leg image is not segmented properly, a manual correction is made. This scheme is better than Su et al.'s method because it considers the inclined leg also. Fig. 2 shows an example. In Fig. 2, the first row shows a region of interest and a segmented image obtained by Su et al.'s method and the second row shows a region of interest and segmented image obtained by proposed scheme. For the proposed scheme, AA' and BB' may not be a horizontal line and the region is defined by a minimum rectangle to include the leg region between AA' and BB'.

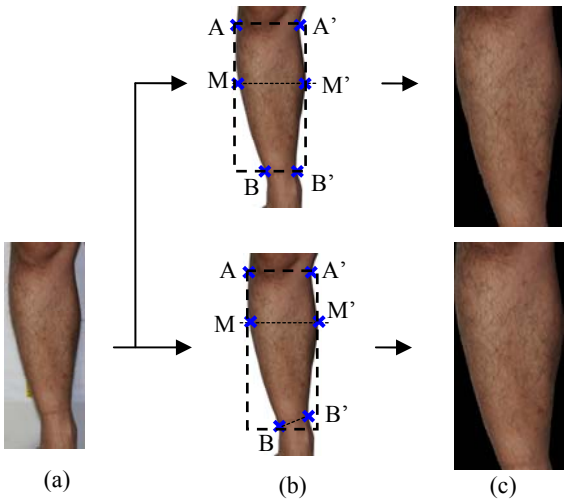

Fig. 2. The preprocessing step. (a) An input image. (b) Region of interest is defined by 6 edge points, A, A', M, M', B and B'. The horizontal distance between M and M' is the longest. The length of AA' is the shortest above MM' and the length of BB' is the shortest below MM'. (c) Preprocessed image is cropped according to the region of interest. The first row is the Su et al.'s method and the second row is the proposed scheme.

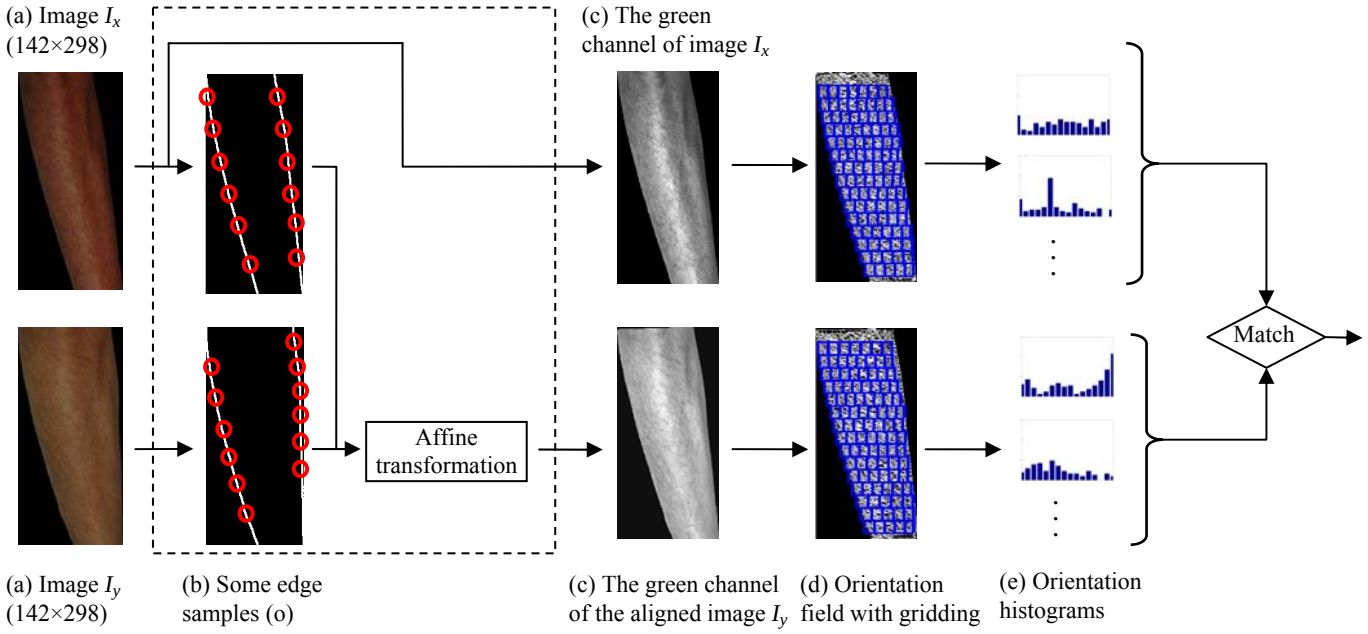

Fig. 3. The schematic diagram of the overall system for low resolution leg identification. It includes the proposed alignment algorithm and the feature matching method in [1]. Note that the dashed region is the proposed alignment algorithm.

III. The Proposed Alignment Algorithm

The proposed alignment algorithm has two components — edge sampling and registration. Fig. 3 shows the schematic diagram of the entire system for identifying criminals and victims based on lower leg images. Since the objective of this paper is to tackle the identification problem in low resolution leg images, all testing images are resized to 142 × 298 pixels (Fig. 3(a)). Next, the edge samples (o) are extracted from an evidence image I_x and a suspect image I_y in a given database (Fig. 3(b)). The images in the suspect database can be collected from criminals in a sex offender registry or ex-prisoners. Then, edge samples are extracted to align the images (Fig. 3(c)). And then, the method reported in [1] is applied to the green channel of the image pair in Fig. 3(c). The green channel is employed because it is the optimal channel for the matching method. In Fig. 3(d), the Gabor orientation field is computed and divided into grids. The orientation histograms can be extracted from each grid (Fig. 3(e)) and a matching distance is calculated based on the orientation histograms. Finally, the matching distance given by the method is used to rank the suspects in the given database.

A. *Edge Sampling*

Edge is a useful clue for image alignment. Directly using all edge points on leg boundaries to perform alignment is not a computationally efficient approach because points near to each other contain similar information. There are many sampling methods. The regular sampling method takes every k^{th} point that is sorted by their *y*-coordinates in an ascending order. It is simple and easy to be implemented, but not rotation invariant, meaning that the method obtains different sample points for an image and its rotated version. Fig. 4 illustrates this problem.

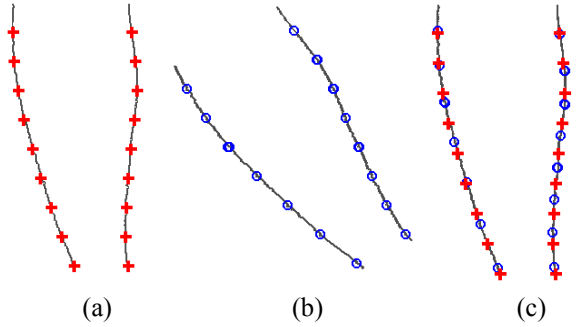

Fig. 4. Illustration of the weakness of the regular sampling method. (a) and (b) are the leg boundaries of the same image. (b) is a rotated version of (a) with 30 degrees difference. The red crosses and blue circles are given by the regular sampling method. (c) The image in (b) is turned back by -30 degrees and then is overlaid with the image in (a).

Figs. 4(a) and (b) show the sample points given by the regular sampling method. The leg boundary in Fig. 4(a) is from an original image and the leg boundary in Fig. 4(b) is from its rotated version. Their difference is 30 degrees. Fig. 4(b) is rotated back and is overlaid with Fig. 4(a). Fig. 4(c) shows the overlaid result. It is obvious that the red crosses and the blue circles in Fig. 4(c) do not match well. The regular sampling method is not rotational invariant. If the images rely on these sample points for alignment, the misalignment can lead to incorrect matching. Therefore, another sampling method is proposed to resolve the misalignment of the sample points.

The proposed scheme makes use of angular sampling to determine the points for alignment. This scheme depends on a center point and a centerline. To estimate the center point, the distance transform [13] defined as

$$D_i(p) = \min_{b \in B_i} \| p\text{-}b \|_2 , \tag{1}$$

where $i \in \{L, R\}$, B_L and B_R are the left and right boundaries of a leg, D_L and D_R are the results from the left and right boundaries, and $p = (x, y)$ is a pixel location of the leg in an input image, is used. To combine information in both boundaries,

$$D_o(p) = \max(D_L(p), D_R(p)) \cdot \mathrm{e}^{-m} , \tag{2}$$

where $m = \lfloor | D_L(p) - D_R(p) | \rfloor$ and $\lfloor \cdot \rfloor$ denotes a floor operator, is used. The center point is defined as $p_c = \arg\max D_o(p)$. If there exists other points p_k such that $D_o(p_k) = D_o(p_c)$, the center point will be defined as one whose *y*-coordinate is the median. If *k* is even, the center point is defined as one whose *y*-coordinate is a $(k/2)^{\text{th}}$ point that is sorted by their y-coordinates in an ascending order. The centerline, which passes through the center point, is determined by the points in the set $\{p_1, \cdots p_i, \cdots, p_H\}$ where $p_i = \arg\max_p D_o(p)$ and *p* is a pixel in the i^{th} row of D_o. Fig. 5 illustrates D_o with the centerline and the center point.

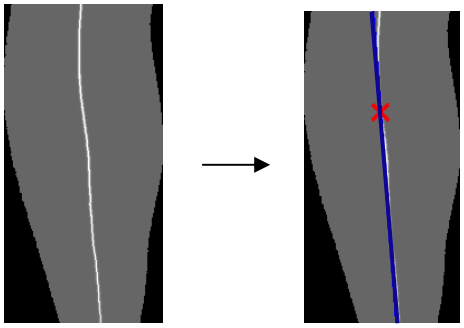

Fig. 5. Illustration of with the centerline and the center point by *Do*. (a) The magnitude map of *Do*. The color is brighter if *Do* is higher. (b) The centerline (Blue line) and the center point (Red cross) are estimated by using *Do*.

Once the center point and the centerline are computed, the points are sampled uniformly in terms of angular distance, illustrated in Fig. 6. In the experiments, 360 sample points were used to represent one image. They were stored as a matrix,

$$\begin{bmatrix} x_0 & x_1 & \cdots & x_{358} & x_{359} \\ y_0 & y_1 & \cdots & y_{358} & y_{359} \end{bmatrix}. \tag{3}$$

In some particular angles, sample points cannot be obtained because the leg boundaries are open. The corresponding values in the matrix are set to zero. The

proposed sampling scheme is applied to the leg boundaries in Figs. 4(a) and (b) and the results are shown in Fig. 6. Clearly, the proposed scheme overcomes the weaknesses of the regular sampling method.

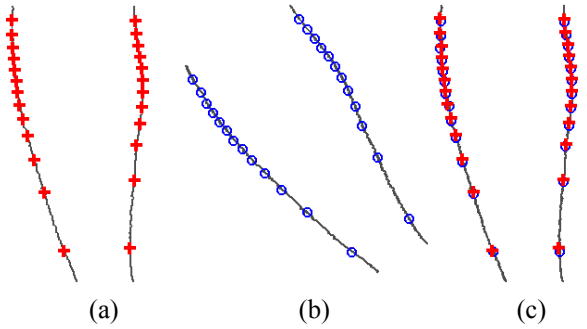

Fig. 6. The proposed sampling scheme is applied to leg boundaries in Fig. 4(a) and Fig. 4(b). (a) and (b) are the corresponding results. (c) The image in (b) is turned back by -30 degree and then is overlaid with (a).

B. Image Registration

To align accurately two input images for matching, the corresponding coordinate matrixes given in Eq. 3 are compared because some sampling angles do not have edge points. A pruning step is used to ensure that every sample can have correspondences for registration. By comparing their coordinate matrixes, the sample points in both matrixes with zero values are removed. Note that the sampling angles are based on the centerline and therefore, this step still keeps the property of rotational invariant.

Then, the sample points are normalized for enhancing translation and scale robustness. Afterwards, the affine coherent point drift (CPD) [12], which utilizes Gaussian mixture models for data modeling and an expectation-maximization method for optimization, is used to align two sets of edge samples. The transformation matrix given by the affine CPD and cubic interpolation are used to project one of the images to the other. Fig. 7 shows some examples of the aligned images.

IV. FEATURE MATCHING

The proposed alignment algorithm uses the feature matching method reported in [1] for identification and evaluation. Thus, a summary of the method is given in this section for completeness. Firstly, Gabor filters are applied to the green channel of an input image. Then, the Gabor orientation field is computed by $O(x,y) = \arg_{\theta_k} \max |G_{\theta_k} * I|$, where G_{θ_k} is a Gabor filter with the orientation θ_k and I is the green channel of the input image. And then, the orientation field is divided into blocks by a dynamic grid system which determines the block sizes based on the width of each row in the leg (Fig. 8).

In the dynamic grid system, the number of blocks in the i^{th} row is obtained by

$$N_i = \left\lfloor \frac{E}{2} \times \frac{\mu_{is}}{\mu_{ia}} + 0.5 \right\rfloor, \quad (4)$$

where $i = 1, \cdots, E$, μ_{is} is the average number of skin pixels in the i^{th} row, μ_{ia} is the total number of pixels in the i^{th} row including background pixels, E is the number of rows to be divided and $\lfloor \cdot \rfloor$ denotes a floor operator. Once the number of blocks is known, the block size can be easily obtained for each row.

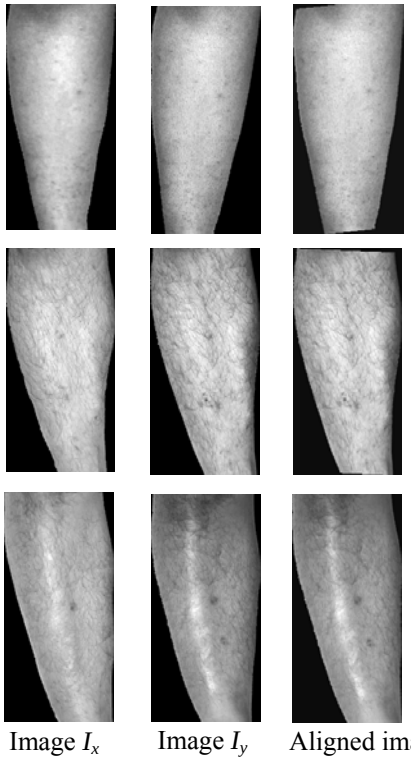

Fig. 7. Some aligned examples from different image pairs by columns. Images in the same row are from the same leg. The first and the second columns are preprocessed input images for alignment. Images in the third column are aligned results.

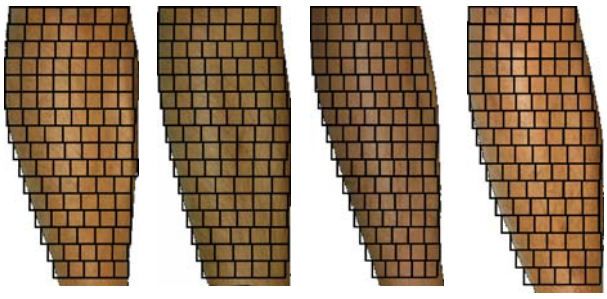

Fig. 8. Illustration of the dynamic grid system in [1]. The block size is determined by the width of each row and each block is represented by a black rectangle.

In each block, the Gabor orientation field is processed to obtain a Gabor orientation histogram. To measure the dissimilarity between the orientation histograms from the two input images, the blockwise Chi-square distance defined as

$$X(H_{O_i}, H_{O_d}) = \sum_{t=1}^{N}\sum_{k=1}^{K} \frac{(h_{O_i B_t}(k) - h_{O_d B_t}(k))^2}{h_{O_i B_t}(k) + h_{O_d B_t}(k)}, \qquad (5)$$

where $H_{O_i} = \{h_{O_i B_1}, ..., h_{O_i B_N}\}$ and $H_{O_d} = \{h_{O_d B_1}, ..., h_{O_d B_N}\}$ are Gabor orientation histograms from the image I_x and an the aligned image I_y, respectively, K is the number of orientation and N is the total number of blocks, is used. Since the first row in the aligned image may not completely appear because of the projection, its blocks are not used for matching. In the experiments, the first row of the blocks is discarded for the sake of fair comparison.

V. Experimental Results

The testing database contained 1,138 leg images from 283 subjects. All the images were captured in two occasions with an interval of around 11 days. In the first occasion, 575 images were captured from the 283 subjects' right legs and in the second occasion, 563 images from the same 283 subjects' right legs were captured. Images collected in the first occasion were considered as a probe set and images collected in the second occasion were considered a gallery set. Fig. 11 shows some samples in the probe set and the gallery set. These two sets contained the frontal view of the legs but their pose and quality were not strictly restricted. Thus, viewpoint, illumination, occlusion and shadow might exist. These testing images were segmented by the method slightly modified from [1], which is mentioned in Section II. The purpose of the experiment was to evaluate the performance of the proposed alignment algorithm on low resolution images. The images in both sets were resized to 142 × 298 pixels. Cumulative Match Characteristic (CMC) curves were used to objectively evaluate the effectiveness the proposed algorithm.

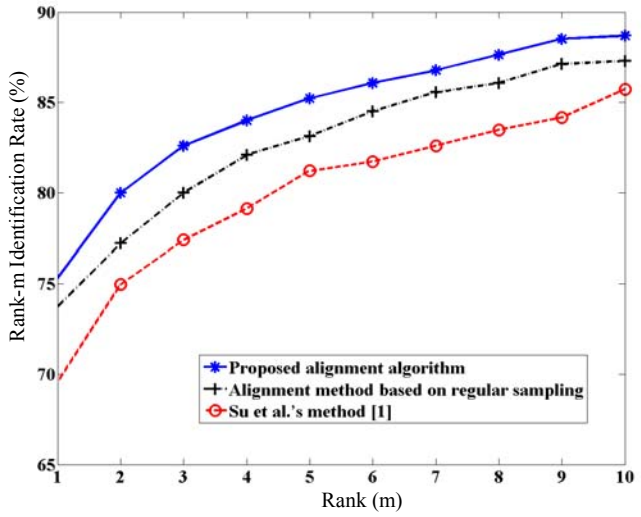

Fig. 9. The CMC curves obtained from different alignment methods. The same feature matching method mentioned in Section IV was used in all the methods.

Fig. 9 shows the CMC curves of Su et al.'s method, the alignment method based on regular sampling and the proposed alignment algorithm. Even though Su et al.'s method and the proposed alignment algorithm use the same feature and matching method, the proposed alignment algorithm can still provide a significant improvement. The rank-1 identification accuracy of the proposed alignment algorithm is 75.3%, while the rank-1 identification accuracy of Su et al.'s method is 69.6%. Besides, a comparison of the CMC curves of the proposed alignment algorithm and the alignment method based on regular sampling demonstrates the effectiveness of the proposed sampling scheme. The rank-1 identification accuracy of the proposed alignment algorithm is 1.56% higher than that of the alignment method based on regular sampling. These experimental results show that the proposed alignment algorithm is effective for alleviating the alignment problem, which was neglected in [1].

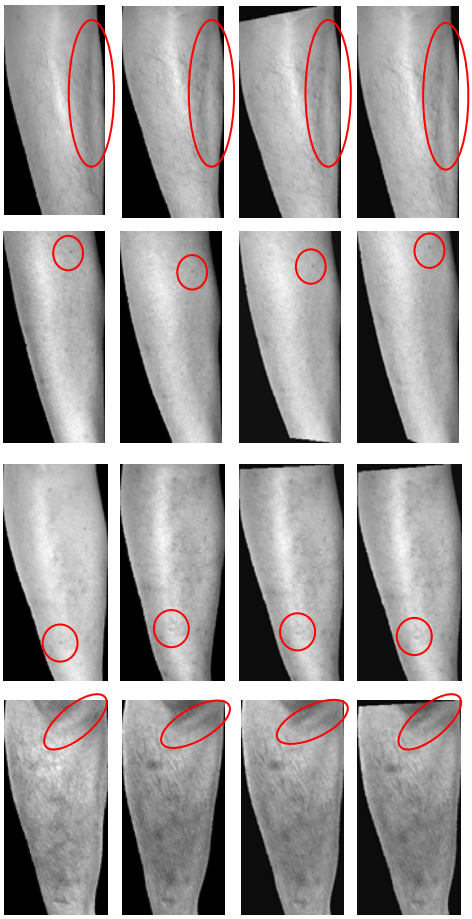

Fig. 10. The alignment results given by different alignment methods. Each row is a set of images from the same leg. The first column is images from the probe set. The second column is the images from the gallery set. The third column is the results from given by the alignment method based on regular sampling and the last column is the results given by the proposed alignment. The results in the last column are obtained by projecting the images in the second column to those in the first column. Note that the results in last column are the most matched one for the images in the first column. The red ellipse is used to show the alignment of the leg by hightlighting some unique textures on the leg.

To further analyze the experimental results, Fig. 10 shows alignment results of four legs given by the alignment method based on regular sampling and the proposed alignment algorithm. Each row is a set of images from the same leg. The first column is images from the probe set. The second column is the images from the gallery set. The third column is the results given by the alignment method based on regular sampling and the last column is the results given by the proposed alignment. The results in the third column and the last column are obtained by projecting the images in the second column to those in the first column. Since Su et al.'s method identifies leg images without alignment, the images in the second column are directly matched with those in the first column. The images of these two columns are quite different and therefore Su et al.'s method cannot match them correctly. The alignment method based on regular sampling cannot align images in the first and the second columns very well. This inaccurate alignment is due to the fact that it takes sample points from every k points on the boundaries, which is not rotational invariant and may not have correct correspondence illustrated in Fig. 4(c). Although the affine CPD method can handle rotation and scale variations, it cannot recover this error and finally an inaccurate alignment is produced. However, when the proposed alignment algorithm is applied to the images in the first and the second columns in Fig. 10, the shapes of the aligned images are more similar to the original images in the first column and the aligned images can be matched to them by using the feature matching method. Since the proposed alignment algorithm chooses the sample points with consideration of rotation variations, the corresponding points can be easily found in the image pairs. Thus, the proposed alignment algorithm can outperform Su et al.'s method and the alignment method based on regular sampling.

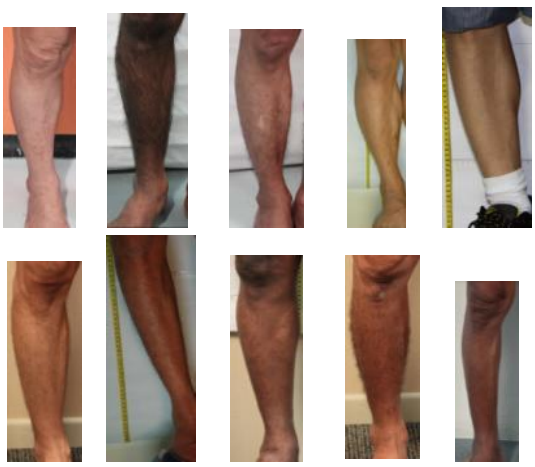

Fig. 11. Some samples in the Image Set 1 and Image Set 2.

VI. Conclusion

To accurately align androgenic hair patterns in low resolution leg images for criminal and victim identification, in this paper, an algorithm based on leg geometry, angular sampling and affine transform is developed. It was examined on a database containing 1,138 leg images from 283 subjects. The experimental results demonstrate that the proposed algorithm outperforms the method proposed by Su et al. [1] and the proposed angular sampling scheme also outperforms the regular sampling scheme. In term of rank-1 identification accuracy, more than 5% improvement is obtained when comparing with Su et al.'s method.

Acknowledgments

We would like to thank the U.S. Department of Justice, the U.S. Immigration and Customs Enforcement, the Singapore Prison Service, and the Singapore Police Force for providing legal and forensic information. This work is partially supported by the Ministry of Education, Singapore through Academic Research Fund Tier 2, MOE2012-T2-1-024.

References

[1] H. Su, and A.W.K. Kong, "An evaluation on low resolution androgenic hair patterns for criminal and victim identification," *IEEE Trans. Inf. Forensics Security*, conditionally accepted.

[2] Canada's National Tipline for Reporting the Online Sexual Exploitation of Children Statistics [Online]. Available: http://www.cybertip.ca/pdfs/fact_sheet_pdfs/English/CyberStats_en.pdf

[3] A. Nurhudatiana, A.W.K. Kong, K. Matinpour, S.Y. Cho, and N. Craft, "Fundamental statistics of relatively permanent pigmented or vascular skin marks for criminal and victim identification," in *Proc. IJCB*, Washington, DC, USA, 2011, pp. 1-6.

[4] C. Tang, A.W.K. Kong, and N. Craft, "Uncovering vein patterns from color skin images for forensic analysis," in *Proc. IEEE CVPR*, Colorado Springs, CO, USA, 2011, pp. 665-672.

[5] K.S. Stenn and R. Paus, "Controls of hair follicle cycling," *Physiological Reviews*, vol. 81, no. 1, pp. 449-491, 2001.

[6] W. Montagna, and R.A. Ellis (eds), *The biology of hair growth*, Academic Press, New York, 1958.

[7] C. Harris, and M. Stephens, "A combined corner and edge detector," in *Proc. of 4th Alvey Vision Conf.*, 1988, pp. 147–151.

[8] D. G. Lowe, "Object recognition from local scale-invariant features," in *Proc. ICCV*, Kerkyra, Greece, pp. 1150-1157, 1999.

[9] Y. Ke and R. Sukthankar, "PCA-SIFT: A more distinctive representation for local image descriptors," in *Proc. IEEE CVPR*, Washington, USA, 2004, pp. 511-517.

[10] H. Bay, A. Ess, T. Tuytelaars, and L.V. Gool, "SURF: speeded up robust features," *Computer Vision and Image Understanding*, vol. 110, no. 3, pp. 346-359, 2008.

[11] J.L. Crowley and F. Berard, "Multi-modal tracking of faces for video communications," in *Proc. IEEE CVPR*, Puerto Rico, 1997, pp. 640-645.

[12] A. Myronenko, and S. Xubo, "Point set registration: coherent point drift," *IEEE Trans. Pattern Anal. Mach. Intell.*, vol. 32, no. 12, pp. 2262-2275, 2011.

[13] C.R. Maurer, R. Qi, and V. Raghavan, "A linear time algorithm for computing exact euclidean distance transforms of binary images in arbitrary dimensions," *IEEE Trans. Pattern Anal. Mach. Intell.*, vol. 25, no. 2, pp. 265-270, 2003.